June 2010 *ISSN : 0974 - 7478* *Volume 6 Issue 1*

Trade Science Inc.

Macromolecules

An Indian Journal

Full Paper

MMAIJ, 6(1), 2010 [6-14]

Preparation, characterization and determination of magnetic properties of ferrofluids using chitosan-coated magnetic nanoparticles and tween 80 as surfactant for hyperthermia application

Thalia Camila Coelho[1], Mauro Cesar Marghetti Laranjeira[1]*, Rogerio Laus[1], Valfredo Tadeu de Fávere[1], Cristiano da Silva Teixeira[2], Mauricio Rigoni[3], Nelson Jhoe Batistela[3]

[1]Departamento de Química, Universidade Federal de Santa Catarina, Campus Universitario, 88040-900 Florianópolis-SC, (BRAZIL)

[2]Departamento de Engenharia Mecanica, Universidade Federal de Santa Catarina, Campus Universitario, 88040-900 Florianopolis-SC, (BRAZIL)

[3]Departamento de Engenharia Eletrica, Universidade Federal de Santa Catarina, Campus Universitario, 88040-900 Florianopolis-SC, (BRAZIL)

E-mail : mauro@qmc.ufsc.br

Received: 15th December, 2009 ; Accepted: 25th December, 2009

ABSTRACT

Magnetite and maghemite nanoparticles were prepared by co-precipitation and oxidation methods, respectively. The magnetic nanoparticles obtained were coated with a layer of the surfactant Tween 80 dispersed in chitosan (CTS) solution. The infrared spectroscopy (IR) analysis confirmed the presence of all functional groups of iron oxides and the thermogravimetric analysis revealed a structural difference between the magnetic nanoparticles. X-ray diffraction (XRD) results of the naked oxides and ferrofluids revealed that the resultant nanoparticles were naked oxides with a spinel structure. Magnetic measurement revealed that the saturated magnetization of the uncoated nanoparticles was higher than that of the coated nanoparticles. All samples were placed within an alternating magnetic field and it was observed that the maximum temperatures obtained for the magnetite, maghemite, magnetite/CTS and maghemite/CTS were 48.3, 49.9, 42.5 and 43.3°C, respectively. Therefore, magnetic nanoparticles do, indeed, appear to be promising as a potential magnetic support for hyperthermic applications.

KEYWORDS

Magnetite;
Maghemite;
Chitosan;
Ferrofluids;
Hyperthermia.

INTRODUCTION

The application of different forms of iron oxides in diagnostic radiology procedures has gained wide acceptance in radiological practice, but therapeutic applications are still under investigation and development.

Such applications exploit two major advantages of magnetic iron oxides: their low toxicity to human beings and the possibility to exploit their outstanding magnetic properties, potentially allowing the use of the high magnetization of superparamagnetic iron oxide to obtain drugs which target the tumor area through external static magnetic fields[1].

Hyperthermia is one of the promising approaches to cancer therapy. This idea is based on the principle that a magnetic particle can generate heat by hysteresis loss under an alternating magnetic field (AMF). Magnetic particles embedded around a tumor site and placed within an oscillating magnetic field will heat up to a temperature dependent on the magnetic properties of the material, the strength of the magnetic field, the frequency of oscillation and the cooling capacity of the blood flow at the tumor site. Cancer cells are destroyed at temperatures higher than 43°C, whereas the normal cells can survive at higher temperatures. Regarding their application in hyperthermia, the important properties of magnetic particles are non-toxicity, biocompatibility, injectability, high-level accumulation in the target tumor, and effective absorption of the energy of AMF. Choosing high-power magnetic particles combined with an appropriate external magnetic field, very small amounts of fine magnetic particles (in the order of tenths of a milligram) can easily be used to raise the temperature of biological tissue locally up to cell necrosis[2,3].

In the last decade, increased investigations with several types of iron oxides have been carried out in the field of nanosized magnetic particles (mostly magnetite, Fe_3O_4, or maghemite, γ-Fe_2O_3, with single domains of about 5–20 nm in diameter), among which magnetite is a very promising candidate since its biocompatibility has already been proven. Magnetite has a cubic inverse spinel structure with oxygen forming an fcc closed packing and Fe cations occupying interstitial tetrahedral sites and octahedral sites[2-4]. Maghemite belongs to the inverse spinel class (A) $[B]O_4$ and exhibits a vacancy-ordered spinel structure, where the vacancies are exclusively located at the octahedral [B] sites. The structure of maghemite can be written as $(Fe^{3+})[Fe^{3+}_{5/3}\square_{1/3}]O_4$[5,6]. Magnetite and maghemite are attracting considerable interest in relation to several biomedical applications; amongst these are therapeutic applications, such as: hyperthermia, magnetic resonance imaging, cell separation techniques, tissue repair, magnetofection and drug release[1,7-13].

Ferrofluids are a new class of magnetic materials comprising a colloidal suspension of magnetic particles coated with a layer of surfactant dispersed in a carrier liquid[7,8]. A stabilizer such as a surfactant or a polymer is usually added at the time of preparation to prevent aggregation of the nanoscale particles[2]. Magnetic carriers can be manufactured using inorganic materials or polymers. In fact, high mechanical resistance, thermal stability, resistance to solvent and microbial attack, ease of manufacture and excellent shelf life make inorganic materials ideal supports, but they have limited functional groups for selective binding. To overcome this problem, magnetic carriers are most commonly manufactured from polymers, since they have a variety of surface functional groups which can be tailored to specific applications. In the literature, different types of natural and synthetic polymers (e.g. chitosan, calcium alginate, polystyrene, polyacrylamide, polyvinyl alcohol, nitrocellulose, and polyvinyl butyral) have been used in the preparation of magnetic carriers[14].

Tweens are probably the most commonly used nonionic surfactants in the pharmaceutical industry. They comprise a partial fatty acid ester of sorbitol-derived cyclic ether, condensed with a fixed, but statistically distributed, number of ethylene oxide units, which gives the product a high degree of heterogeneity. Tween 80 is specifically an industrial "oleic acid" ester (with ~30% non-oleic chains) conjugated with approximately 20 ethylene oxide units per molecule. Tween 80 is very soluble in water and soluble in ethanol. It is employed to stabilize or solubilize agents in medicinal, pharmaceutical and cosmetic product preparations, and is a well-established food additive, owing to its attractive cost and relatively low toxicity[15,16].

Chitosan can be used as a base material for magnetic carriers. It is a polyaminosaccharide, β-(1-4)-2-amino-2-deoxy-D-glucopyranose, which contains high contents of amino and hydroxyl groups[17-19]. Chitosan offers important properties, such as abundance, nontoxicity, hydrophilicity, biocompatibility, biodegradability, antibacterial properties and a remarkable affinity for many biomacromolecules[20-24]. Chitosan can be pro-

duced by alkaline deacetylation of chitin, one of the most abundant biopolymers in nature[25-27]. It has several potential applications in the areas of biotechnology, biomedicine, food processing, cosmetics, wastewater treatment, metal chelating agents and other industrial applications[20,21,28-32].

In this study, iron oxide magnetic particles were coated with the surfactant Tween 80, to prevent aggregation of the magnetic nanoparticles, and chitosan to exert two important functions in the preparation of ferrofluids: to coat the iron oxides in order to avoid damage to normal cells and as a dispersant. Here, we report the use of new ferrofluids to be applied in cancer treatment. The materials were characterized through infrared spectroscopy (IR), X-ray diffraction (XRD), flame atomic absorption spectrometry (FAAS), thermogravimetric analysis (TGA), differential scanning calorimetry (DSC) and vibrating sample magnetometer (VSM) for hyperthermia application.

EXPERIMENTAL

Reagents

Chitosan (CTS, MW 122.74 kDa, degree of deacetylation 90%) was purchased from Purifarma Company (Sao Paulo, Brazil). Ferric nitrate nonahydrate, ferric chloride hexahydrate and ferrous chloride tetrahydrate were purchased from Fluka, Synth and Sigma-Aldrich, respectively. Ammonia, nitric acid and Tween 80 were purchased from Dinâmica, Sigma-Aldrich and Synth, respectively. Working standard solutions of iron(III) ions were prepared using the appropriate dilution of a 1000mg L^{-1} stock solution of the respective analyte (Merck, Darmstadt, Germany). Other chemicals were of analytic grade and used without further purification. All solutions were prepared with deionized water.

Apparatus

Infrared spectra were obtained with KBr discs in the range of 4000 to 400cm^{-1}, using a spectrometer with a Fourier Transform System (Perkin Elmer 16 PC). XRD analysis was carried out using a X-ray powder diffractometer (Philips X'Pert) with $CuK_{\alpha 1}$ radiation (λ=1.54056 A°), the X-ray generator operating at 40 kV and 30mA. A continuous scan mode was used to collect 2θ data from 10 to 80°. Nanoparticle size was calculated using the half width of the XRD diffraction line. TGA and DSC were carried out using a Shimadzu TGA 50 and a Shimadzu DSC 50, respectively. Both analytical techniques were carried out with a heating rate of 10°C min^{-1}, under nitrogen atmosphere flowing at a rate of 50mL min^{-1}. DSC curves were obtained from the first heating runs. The concentration of iron was determined by FAAS using a Varian Spectra 50 spectrometer equipped with an air-acetylene flame atomizer and Hitachi hollow cathode lamp specific for iron. The lamp current was 5mA, the slit width was 0.2 nm, the wavelength was 248.3 nm and the aspiration rate was 6mL min^{-1}. The magnetic properties of the particles were assessed with a VSM LD 9600 in terms of saturation magnetization. The temperatures to which samples were heated on application of an alternating magnetic field were recorded. The experiments were carried out at 25°C within an induced heating system composed of a solenoid with diameter of 25.5mm, length of 150mm and 102 spirals, fed to a frequency inverter with a feeding frequency of 24.7 kHz and magnetic field amplitude of 3.2kA m^{-1} (Figure 1). The samples were placed in a test tube that was coupled to a heating system, and the temperature was measured by an alcohol thermometer in order to avoid any interference with the magnetic field.

Preparation of magnetite nanoparticles by co-precipitation method

Magnetite was precipitated by mixing 2.08g $FeCl_2.4H_2O$ and 5.22g $FeCl_3.6H_2O$ in 380mL of deionized water and adding 20mL 25% NH_4OH dropwise, under vigorous stirring and nitrogen atmosphere. The

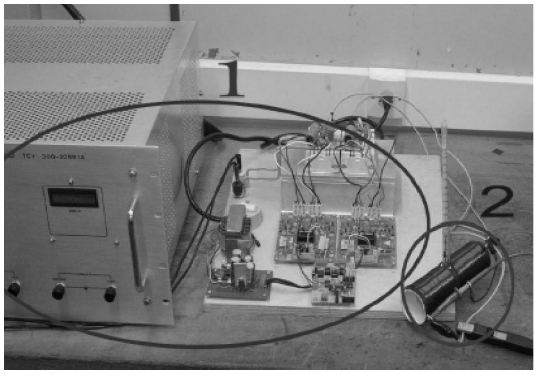

Figure 1 : Heating system composed of a frequency inverter (1) and solenoid (2)

black precipitate was formed immediately and separated from the remaining solution, washed several times with deionized water until neutral pH and dried at room temperature, to avoid the oxidation of magnetite.

Preparation of maghemite nanoparticles by oxidation of magnetite

Maghemite was prepared by oxidation of the magnetite using 40mL of 2.0 mol L^{-1} HNO_3 with vigorous stirring for 5 min. To complete the oxidation, 60mL of 0.35 mol L^{-1} $Fe(NO_3)_3$ was added and the solution was heated until boiling, which was maintained for 1 h. The brown precipitate was separated from the remaining solution, washed several times with deionized water and dried at room temperature.

Preparation of ferrofluids with magnetite and maghemite nanoparticles

The ferrofluids were prepared by mixing 300 mg of magnetic nanoparticles (magnetite or maghemite) and approximately 0.2mL of Tween 80. To this mixture 30mL 1.5% (w/v) of chitosan dissolved in 1.0% (v/v) acetic acid solution was added to disperse the magnetic particles and the mixture was kept under agitation. Subsequently, the pH was increased to 5.5 with addition of 5 mol L^{-1} NaOH solution, since the acidic medium is toxic for studies *in vivo*. The solid was filtered, washed with deionized water and dried at room temperature.

Determination of iron in magnetic nanoparticles by FAAS

To determine the amount of iron in the magnetic nanoparticles approximately 10.0mg of each sample was dissolved in 50mL of 2.0 mol L^{-1} HCl. Aliquots (250μL) were removed and diluted to an adequate volume to determine the concentration of iron by FAAS. The tests were performed in triplicate.

RESULTS & DISCUSSION

Infrared spectroscopy

The IR spectra of the magnetite, maghemite, Tween 80, CTS, magnetite/CTS and maghemite/CTS are shown in figure 2.

Figure 2a shows the spectrum for magnetite. The characteristic absorption bands at 628 and 588cm^{-1}

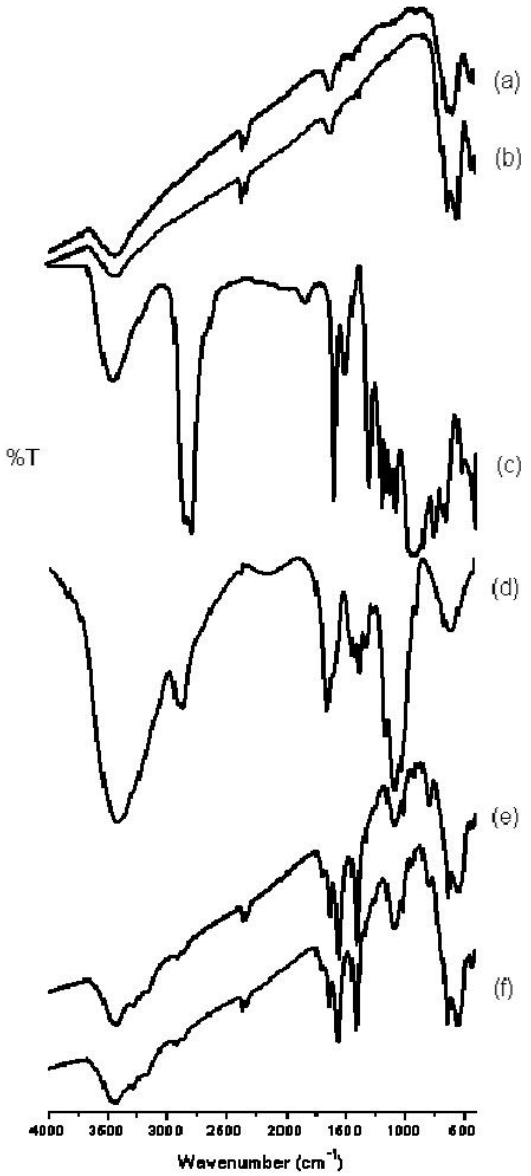

Figure 2 : Infrared spectra of: (a) magnetite, (b) maghemite, (c) Tween 80, (d) CTS, (e) magnetite/CTS and (f) maghemite/CTS

were assigned to Fe-O deformation in the octahedral and tetrahedral sites, while the band at 451cm^{-1} refers only to Fe-O deformation at octahedral sites. Some notable absorption bands appearing at 3431 and 1620cm^{-1} were assigned to the O-H stretching vibration and H-O-H bending vibration, respectively.

The infrared spectrum of maghemite (Figure 2b) was rather similar to that of magnetite, since the same functional groups were present in the two types nanoparticles. Therefore, the same vibrations were observed with different relative intensities.

Figure 2c shows the spectrum of Tween 80 which shows a band at 3482cm^{-1} corresponding to the O-H

stretching vibration and bands at 2924 and 2862cm^{-1} were assigned to the C-H stretching vibration. The peak at 1735cm^{-1} was attributed to the C=O axial deformation. The peak at 1642cm^{-1} was attributed to the C=C axial deformation. The bands at 1457 and 1348cm^{-1} were attributed to the C-H asymmetric and symmetric bending deformation of the CH_2 groups. The peak at 1324cm^{-1} was attributed to the C-O stretching vibration. The band at 1291cm^{-1} was associated with the C-O-C asymmetric stretching vibration, whereas bands at 1100 and 993cm^{-1} were attributed to the C-O-C symmetric stretching vibration. The peak at 845cm^{-1} was attributed to the O-H out-of-plane bending deformation.

Chitosan (Figure 2d) depicted an intense absorption band at 3439cm^{-1} corresponding to the O-H stretching vibration, whereas bands at 2930 and 2880cm^{-1} were assigned to the C-H stretching vibration. In addition, bands at 1655 and 1602cm^{-1} were associated with the C=O stretching vibration of secondary amide groups and the N-H deformation vibration of primary amine, respectively. The band at 1381cm^{-1} was attributed to the C-H deformation of the CH_3 group, associated with the few remaining acetamide groups present in the polymeric chain, as a result of the incomplete deacetylation of chitosan. Finally, there was a band at 1081cm^{-1} corresponding to the C-O stretching vibration of the primary alcohol[17].

Figure 2e (magnetite/CTS) shows a band at 3431cm^{-1} corresponding to the O-H stretching vibration. In addition, bands at 3284 and 3166cm^{-1} were associated with O-H deformation vibrations and a C-H asymmetric stretching vibration, respectively. Bands at 2930 and 2863cm^{-1} were assigned to the C-H stretching vibration. In addition, a band at 1705cm^{-1} was attributed to the C=O axial deformation of Tween 80. The peak at 1638cm^{-1} was attributed to the C=O stretching vibration of secondary amide groups. At 1557cm^{-1} a new band was observed, which can be attributed to the ionic interaction between the positively charged amine groups of CTS and the negatively charged carbonyl groups of Tween 80[33]. The peak at 1413cm^{-1} corresponded to the C-H bending deformation. The peak at 1093cm^{-1} was attributed to the C-O-C symmetric stretching vibration of Tween 80 or C-O stretching vibration of the primary alcohol. A band at 805cm^{-1} was attributed to the ethyl chain axial vibration. Finally, the bands at 639 and 558cm^{-1} are assigned to Fe-O deformation in the octahedral and tetrahedral sites. The iron atoms of the magnetic particles are probably coordinated to the nitrogen atoms of deprotonated amino groups in chitosan since at pH 5.5 the polymeric chain of chitosan shows approximately 10% of deprotonated amino groups[34].

No significant differences were noted on comparing the spectrum of maghemite/CTS (Figure 2f) with that of magnetite/CTS, thus the same vibrations were observed with different relative intensities.

The results indicated that the surfactant and polymer had coated the magnetic nanoparticles, due to the presence of characteristic bands of materials from the spectra of coated magnetic nanoparticles, besides the presence of a new band.

X-ray diffraction

Figure 3 shows the XRD patterns for the magnetite, maghemite, magnetite/CTS and maghemite/CTS. The XRD results of the naked oxides and ferrofluids were mostly coincident. Six characteristic peaks for magnetite (2θ=30.4, 35.8, 43.2, 53.9, 57.4, and 62.7°), marked by their indices ((220), (311), (400), (422), (511), and (440)), were observed for all samples. These peaks are consistent with the database in the JCPDS file for magnetite and maghemite (PDF No. D021035 and D040755, respectively) and reveal that the resultant nanoparticles were naked oxides with a spinel structure. The presence of these peaks also indicates that the coating process did not result in the phase change of naked oxides. These results verified that the ferrofluids were naked oxides[20,21,35].

Determination of particle size of the magnetic nanoparticles

The size of the magnetic materials can be calculated from the line broadening on the XRD pattern using the Debye–Scherrer equation:

$$\mathbf{d} = \frac{\mathbf{k}\lambda}{\beta \cos\theta}$$

In this equation d is the thickness of the crystal, k is the Debye–Scherrer constant (0.89), λ is the X-ray wavelength, β is the line broadening (in radians) ob-

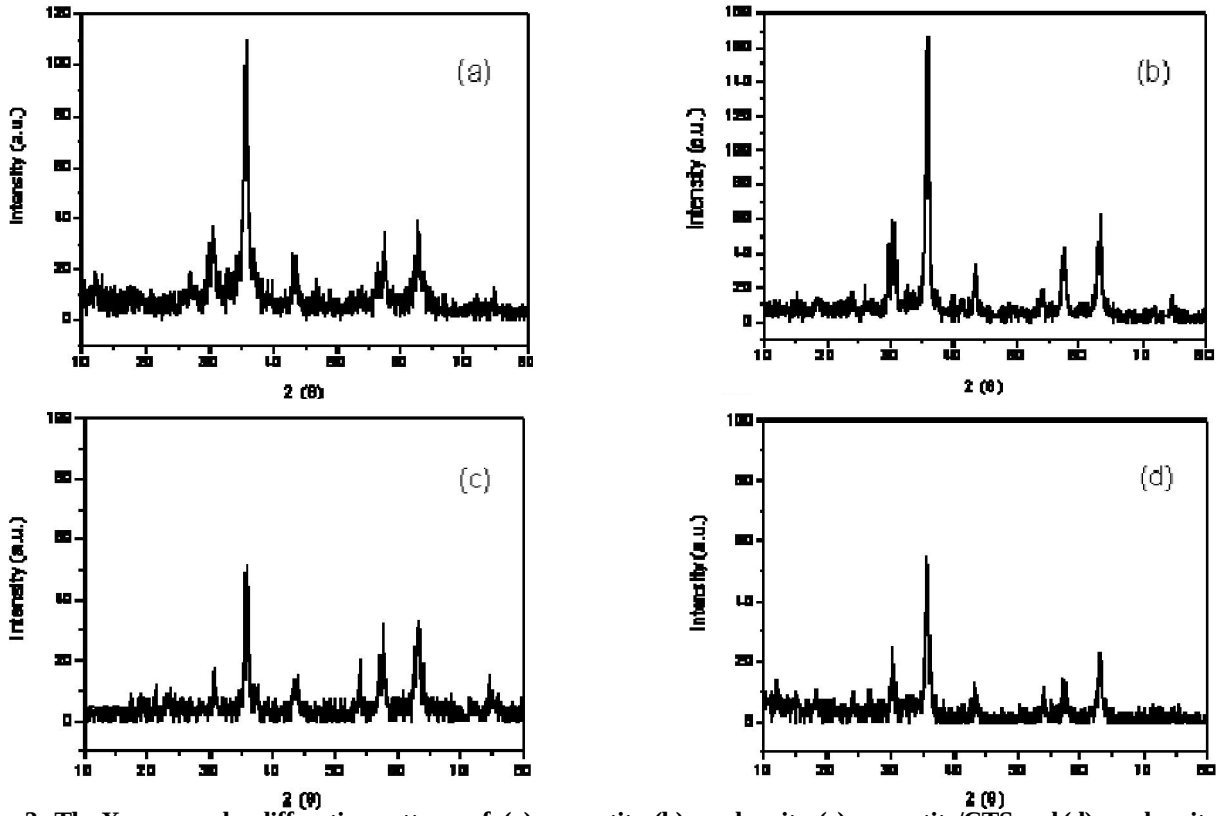

Figure 3 : The X-ray powder diffraction patterns of: (a) magnetite, (b) maghemite, (c) magnetite/CTS and (d) maghemite/CTS

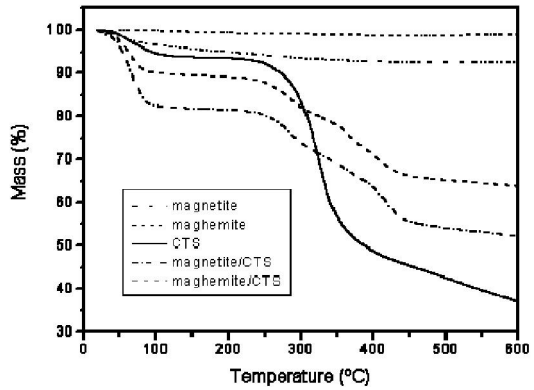

Figure 4 : TGA thermograms of magnetite, maghemite, CTS, magnetite/CTS and maghemite/CTS

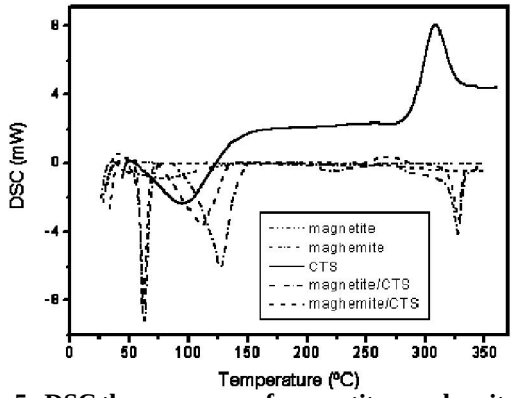

Figure 5 : DSC thermograms of magnetite, maghemite, CTS, magnetite/CTS and maghemite/CTS

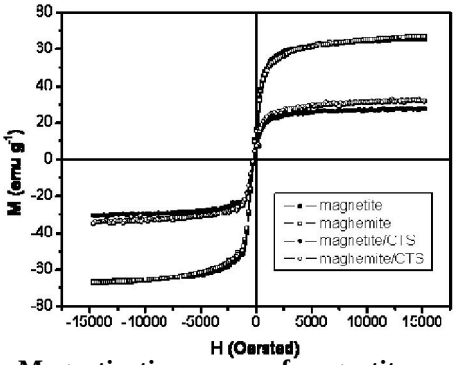

Figure 6 : Magnetization curves of magnetite, maghemite, magnetite/CTS and maghemite/CTS

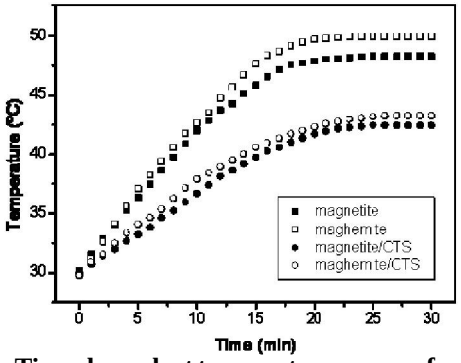

Figure 7 : Time-dependent temperature curves of magnetite, maghemite, magnetite/CTS and maghemite/CTS

tained from the full width at half maximum and θ is the Bragg angle[35].

TABLE 1 shows the values for the particle size of the magnetic materials calculated according to the Debye–Scherrer equation.

Determination of iron in magnetic nanoparticles by FAAS

TABLE 2 presents the experimental values obtained for the magnetite and maghemite as well as for the ferrofluids. It can be observed that the percentages of iron in samples of magnetite/CTS and maghemite/CTS were significantly lower when compared with the samples of maghemite and magnetite, confirming the coating by the surfactant and polymer.

Thermal analysis

The thermal behavior of magnetite, maghemite, CTS, magnetite/CTS and maghemite/CTS was analyzed by TGA and DSC. The thermogravimetric profiles are shown in Figure 4 and they revealed two stages of mass loss. The first degradation stages from around 47-69°C, with a mass loss of 1-18%, are related mainly to the loss of water physically adsorbed on the surface of the materials. In the second stage, other mass losses were observed. The magnetite undergoes a mass loss of 2.96%, at 241.5°C, while the maghemite undergoes mass loss in two stages, at 156.6 and 360.7°C, with losses of 0.43 and 0.60%, respectively. The second degradation stage of chitosan was observed at 332.2°C with a mass loss of 49.68%. The magnetite/CTS shows mass loss in two stages, at 286.8 and 420.7 ºC, with losses of 11.32 and 18.14%, respectively. The maghemite/CTS undergoes mass losses of 9.53 and 15.91%, at 284.9 and 408.7°C, respectively. The degradation temperatures of the materials were established from the first derivative of the thermogravimetric plots.

In figure 5 the DSC thermograms of magnetite, maghemite, CTS, magnetite/CTS and maghemite/CTS can be observed. The DSC thermograms of the magnetite and maghemite showed a small endothermic peak at around 80°C relating to water physically adsorbed on the surface of the materials. The DSC thermogram of chitosan showed an endothermic peak at 103.0°C and an exothermic peak at 308.6°C. In the DSC thermogram of magnetite/CTS three endothermic peaks can be observed, at 62.3, 126.2 (attributed to the water contained on the surface of the materials) and 327.7C (relating to the thermal decomposition of the materials). The maghemite/CTS showed a thermal behavior very similar to magnetite/CTS, also displaying three endothermic peaks, at 61.4, 111.0 and 327.7°C.

The results of the TGA and DSC analysis revealed a structural difference between the magnetic nanoparticles, and confirmed the coating of the naked oxides by the surfactant and polymer.

Magnetic properties

The magnetic properties of the nanoparticles were investigated by VSM analysis.

The magnetic moments of the nanoparticles rapidly saturated in the presence of an externally applied magnetic field, which was varied from 15000 Oe to -15000 Oe. The initial slope of the magnetization curve is relatively steep, indicating superparamagnetic behavior. This signifies that the nanoparticles have essentially single domains, and that they may be ideal component vehicles for magnetic field-directed delivery of therapeutic agents[36].

Figure 6 shows the magnetization curves of magnetite, maghemite, magnetite/CTS and maghemite/CTS.

The magnetic measurements showed that the saturated magnetization values for the magnetite and maghemite were 65.8 and 66.7emu g^{-1}, respectively, while for magnetite/CTS and maghemite/CTS they were 27.7 and 32.1emu g^{-1}, respectively. The decrease in the saturation magnetization for the coated nanoparticles was due to the incorporation of the polymer in the magnetic nanoparticle suspension, since the volume used

TABLE 1 : Particle size of magnetic materials

Samples	Particle size (nm)
magnetite	12.9
maghemite	15.4
magnetite/CTS	13.6
maghemite/CTS	17.2

TABLE 2 : Flame atomic absorption spectrometry results for uncoated and coated magnetic iron oxide particles

Samples	Obtained mass of iron (mg) ± SD	% iron ± SD
magnetite	6.32 ± 0.06	60.19 ± 0.56
maghemite	6.53 ± 0.10	66.00 ± 0.99
magnetite/CTS	1.55 ± 0.02	15.06 ± 0.20
maghemite/CTS	2.64 ± 0.01	26.90 ± 0.08

for the measurement of magnetic properties was the same for all samples.

The decrease in the saturation magnetization can most likely be attributed to the presence of Tween 80 on the surface of the magnetic nanoparticles, which may create a magnetically dead layer. With a significant fraction of surface atoms, any crystalline disorder within the surface layer may also lead to a significant decrease in the saturation magnetization of nanoparticles[35].

Magnetite particles obtained under different synthetic conditions may display large differences regarding their magnetic properties. These differences are attributed to changes in the structural disorder, the creation of antiphase boundaries, or the existence of a magnetically dead layer at the particle surface[2].

Effect of heating temperature as a function of time for iron oxide magnetic particles and ferrofluids

The temperature variation over time for iron oxide magnetic particles and ferrofluids, with the application of an alternating magnetic field, is shown in Figure 7. It can be observed that initially the heating was fast, which makes these materials very interesting from a biological point of view, because their use for cancer treatment will not affect the healthy cells, since the time of exposure to the magnetic field is shorter.

The results also showed that the maximum temperatures obtained for magnetite and maghemite were 48.3 and 49.9°C, respectively, while for magnetite/CTS and maghemite/CTS they were 42.5 and 43.3°C, respectively. The values obtained for the ferrofluids can be considered as very good, since the cancerous cells perish at around 43°C while normal cells are not damaged at even higher temperatures and, thus, ferrofluids could be applied in hyperthermia treatments.

CONCLUSIONS

Ferrofluids were prepared by applying a coating of Tween 80 dispersed in chitosan solution onto the surface of magnetite and maghemite nanoparticles which were prepared by co-precipitation and oxidation methods, respectively.

The coating of surfactant and polymer onto the magnetic nanoparticles was confirmed through infrared spectroscopy, X-ray diffraction, flame atomic absorption spectrometry, thermogravimetric analysis and differential scanning calorimetry.

The magnetic measurements revealed that the saturated magnetization values of the magnetite, maghemite, magnetite/CTS and maghemite/CTS were 65.7, 66.7, 27.7 and 32.1emu g^{-1}, respectively.

After exposure to an alternating magnetic field for 30 min, the temperatures of suspensions containing magnetite, maghemite, magnetite/CTS and maghemite/CTS were 48.3, 49.9, 42.5 and 43.3°C, respectively.

It is expected that magnetic particles will be increasingly applied in biomedicine and will be used to solve many complex problems encountered in cancer diagnosis and therapy in the near future.

ACKNOWLEDGEMENT

The authors wish to thank CAPES-Brazil for financial support.

REFERENCES

[1] A.P.Fink, M.Chastellain, L.J.Jeanneret, A.Ferrari, H.Hofmann; Biomaterials, **26**, 2685 **(2005)**.
[2] AK.Gupta, M.Gupta; Biomaterials, **26**, 3995 **(2005)**.
[3] Z.Ma, H.Liu; China Particuology, **5**, 1 **(2007)**.
[4] K.Hayashi, W.Sakamoto, T.Yogo; J.Magn. Magn.Mater., **321**, 450 **(2009)**.
[5] M.Drofenik, M.Kristl, D.Makovec, Z.Jaglicic, D.Hanzel; Ultrason.Sonochem., **15**, 791 **(2008)**.
[6] J.Mürbe, A.Rechtenbach, J.Topfer; Mater. Chem.Phys., **110**, 426 **(2008)**.
[7] K.Donadel, M.D.V.Felisberto, M.C.M.Laranjeira; An.Acad.Bras.Cienc., **81**, 1 **(2009)**.
[8] K.Donadel, M.D.V.Felisberto, V.T.Fávere, M.Rigoni, N.J.Batistela, M.C.M.Laranjeira; Mater.Sci.Eng.C, **28**, 509 **(2008)**.
[9] R.A.Ali-zade; Colloids Surf.A, **255**, 111 **(2005)**.
[10] D.H.Kim, S.H.Lee, K.H.Im, K.N.Kim, K.M.Kim, I.B.Shim, M.H.Lee, Y.K.Lee; Curr.Appl.Phys., **6S1**, e242 **(2006)**.
[11] D.Y.Lee, Y.I.Oh, D.H.Kim, K.M.Kim, K.N.Kim, Y.K.Lee; IEEE Trans.Magn., **40**, 2961 **(2004)**.
[12] Y.Boguslavsky, S.Margel; J.Colloid Interface Sci., **317**, 101 **(2008)**.

Full Paper

[13] M.A.G.Soler, G.B.Alcantara, F.Q.Soares, W.R.Viali, P.P.C.Sartoratto, J.R.L.Fernandez, S.W.Silva, V.K.Garg, A.C.Oliveira, P.C.Morais; Surf.Sci., **601**, 3921 **(2007)**.
[14] E.B.Denkbaş, E.Kiliçay, C.Birlikseven, E.Ozturk; React.Funct.Polym., **50**, 225 **(2002)**.
[15] S.I.Simoes, J.M.Tapadas, C.M.Marques, M.E. M.Cruz, M.B.F.Martins, G.Cevc; Eur.J. Pharm.Sci., **26**, 307 **(2005)**.
[16] M.Ema, H.Hara, M.Matsumoto, M.H.Koizumi, A.Hirose, E.Kamata; Reprod.Toxicol., **25**, 89 **(2008)**.
[17] T.C.Coelho, R.Laus, A.S.Mangrich, V.T.Fávere, M.C.M.Laranjeira; React.Funct.Polym., **67**, 468 **(2007)**.
[18] F.S.Kittur, K.V.H.Prashanth, K.U.Sankar, R.N.Tharanathan; Carbohydr.Polym., **49**, 185 **(2002)**.
[19] M.S.Chiou, H.Y.Li; Chemosphere, **50**, 1095 **(2003)**.
[20] L.Zhou, Y.Wang, Z.Liu, Q.Huang; J.Hazard.Mater., **161**, 995 **(2009)**.
[21] Y.C.Chang, D.H.Chen; J.Colloid Interface Sci., **283**, 446 **(2005)**.
[22] H.L.Vasconcelos, V.T.Fávere, N.S.Gonçalves, M.C.M.Laranjeira; React.Funct.Polym., **67**, 1052 **(2007)**.
[23] F.C.Wu, R.L.Tseng, R.S.Juang; Water Res., **35**, 613 **(2001)**.
[24] M.N.V.R.Kumar; React.Funct.Polym., **46**, 1 **(2000)**.
[25] J.Fangkangwanwong, R.Yoksan, S.Chirachanchai; Polymer, **47**, 6438 **(2006)**.
[26] W.S.W.Ngah, A.Kamari, Y.J.Koay; Int.J.Biol. Macromol., **34**, 155 **(2004)**.
[27] Q.Wang, N.Zhang, X.Hu, J.Yang, Y.Du; Eur.J.Pharm.Biopharm., **66**, 398 **(2007)**.
[28] A.H.Chen, S.C.Liu, C.Y.Chen, C.Y.Chen; J.Hazard.Mater., **154**, 184 **(2008)**.
[29] E.Guibal; Sep.Purif.Technol., **38**, 43 **(2004)**.
[30] A.J.Varma, S.V.Deshpande, J.F.Kennedy; Carbohydr.Polym., **55**, 77 **(2004)**.
[31] R.Laus, R.Geremias, H.L.Vasconcelos, M.C.M. Laranjeira, V.T.Fávere; J.Hazard.Mater., **149**, 471 **(2007)**.
[32] S.H.Lim, S.M.Hudson; Carbohydr.Res., **339**, 313 **(2004)**.
[33] R.Laus, M.C.M.Laranjeira, A.O.Martins, V.T.Fávere, R.C.Pedrosa, J.C.Benassi, R.Geremias; Quim.Nova, **29**, 34 **(2006)**.
[34] R.Schmuhl, H.M.Krieg, K.Keizer; Water SA, **27**, 1 **(2001)**.
[35] G.Y.Li, Y.R.Jiang, K.L.Huang, P.Ding, J.Chen; J.Alloys Compd., **466**, 451 **(2008)**.
[36] Z.Huang, F.Tang, L.Zhang; Thin Solid Films, **471**, 105 **(2005)**.